Applied Catalysis B: Environmental 111–112 (2012) 536–544

Contents lists available at SciVerse ScienceDirect

Applied Catalysis B: Environmental

journal homepage: www.elsevier.com/locate/apcatb

Hydrogen from ethylene glycol by supercritical water reforming using noble and base metal catalysts

D.J.M. de Vlieger[a], A.G. Chakinala[b,*], L. Lefferts[a], S.R.A. Kersten[b], K. Seshan[a], D.W.F. Brilman[b]

[a] Catalytic Processes and Materials (CPM), Faculty of Science and Technology, IMPACT Research Institute, University of Twente, P.O. Box 217, 7500 AE Enschede, The Netherlands
[b] Thermo-Chemical Conversion of Biomass (TCCB), Faculty of Science and Technology, IMPACT Research Institute, University of Twente, P.O. Box 217, 7500 AE Enschede, The Netherlands

ARTICLE INFO

Article history:
Received 8 September 2011
Received in revised form 28 October 2011
Accepted 1 November 2011
Available online 7 November 2011

Keywords:
Sustainable
Renewable
Supercritical water
Reforming
Hydrogen
Catalysts
Ethylene glycol

ABSTRACT

Catalytic reforming of ethylene glycol (5 and 15 wt%) in supercritical water (450 °C and 250 bar) in the presence of alumina supported mono- and bi-metallic catalysts based on Ir, Pt and Ni was studied. Pt catalyst showed the highest hydrogen yields compared to Ir and Ni. Varying the Pt loading (0.3–1.5 wt%) showed that the intrinsic reforming activities improved with decreasing Pt loadings. However, a lower Pt loading had a large negative effect on the H_2 selectivity and catalyst stability. It was found that the presence of Ni in a Pt–Ni bimetallic catalyst improved hydrogen yields by suppressing methane formation. Moreover, the presence of Ni also enhanced catalyst stability. Results reported here were obtained at WHSV of 18 h^{-1}. The Pt–Ni/Al_2O_3 having a total metal loading of 1.5 wt% (molar ratio Pt:Ni = 1), is identified as a promising catalyst for the reforming of ethylene glycol in supercritical water and may prove suitable for various other SCWG applications.

1. Introduction

Currently, hydrogen is mostly produced by the steam reforming of natural gas and other fossil feedstocks. Hydrogen is widely used in the ammonia industry, oil refining and food industry. It is foreseen that the demand for hydrogen will increase in the future for bio-refinery applications [1–3]. A concept for integrated hydrogen production from aqueous wastes from the bio-refinery is proposed in Fig. 1. In order to meet the projected hydrogen demands more sustainably, hydrogen from bio-renewable organic sources is an elegant solution. This also helps mitigate the environmental concerns associated with the use of the depleting fossil fuel reserves.

The conversion of the aqueous bio/organic wastes (>80% water) into high heating value products such as hydrogen, syngas (CO/H_2) and methane using conventional reforming processes at lower pressures is energy intensive due to the need for the evaporation of water. Currently, two efficient ways of converting the low heating value aqueous wastes are reported [4–6].

First is the so called "aqueous phase reforming" (APR) developed by Dumesic et al. [4,7,8], in which the oxygenate feeds are reacted at mild temperatures in pressurized liquid water (225–265 °C, 29–56 bar) over supported metal catalysts. Disadvantages of this process include: (i) relatively low reactant concentrations have to be used; (ii) a high contact time is required to achieve complete conversion and (iii) sensitivity of catalysts to deactivation because of char/coke formation.

Supercritical water gasification (SCWG) is another process, wherein the properties of supercritical water are exploited for the reforming of organics in the aqueous stream into gaseous products [5,9–11]. At sub- and near critical conditions (*T*: 375 °C, *P*: 220 bar), thermodynamics favor selectivities towards alkanes in preference to hydrogen [12]. Higher temperatures above 600 °C are required to enhance hydrogen formation. Therefore, the need for catalyst arises to steer the product gas selectivities towards hydrogen and to achieve complete carbon to gas conversion at near critical conditions.

Catalysts for APR and SCWG should be active for C–C bond scission in order to be able to decompose the organic molecules and they should further enhance the water gas shift (WGS, $CO + H_2O \rightarrow CO_2 + H_2$) reaction to maximize hydrogen yields. Methanation ($CO_x + (2+x)\ H_2 \rightarrow CH_4 + xH_2O$) and Fischer Tropsch ($CO + 2H_2 \rightarrow -CH_2- + H_2O$) are undesired side reactions, as they consume the desired product, H_2. In order to suppress these reactions, catalysts should not be active for the scission of C–O bond [13]. Lower alkane selectivities are therefore expected for catalysts with low affinity towards C–O bond scission.

In 2003, Davda et al. [13] reported the relative activities of different metals for C–C bond breaking, C–O bond activation, and WGS

* Corresponding author. Tel.: +31 53489 4635; fax: +31 53489 4738.
E-mail address: a.g.chakinala@gmail.com (A.G. Chakinala).

0926-3373/$ – see front matter © 2011 Elsevier B.V. All rights reserved.
doi:10.1016/j.apcatb.2011.11.005

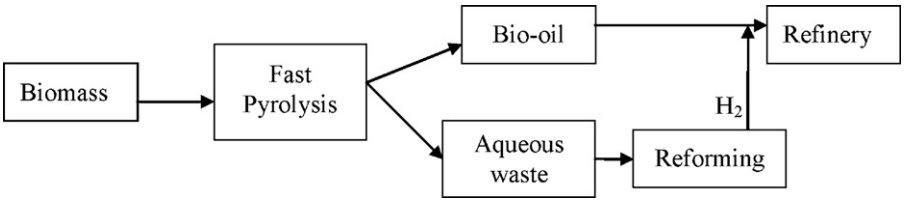

Fig. 1. Integrated hydrogen production and in use for bio-refinery.

reaction. They reported that Ru, Ir and Ni showed high activities for C–C bond breaking, further Ru and Ni metals showed high activities for methane formation. Ir showed very low methanation activity but in contrast to Ru and Ni, almost no WGS activity was reported. Ir is a promising catalyst for breaking down oxygenated hydrocarbons *via* C–C bond scission. Adsorbed oxygenate fractions on the catalyst surface resulting from C–C bond scission undergo dehydrogenation, yielding H_2 and CO [13]. Davda et al. [14] concluded that for the APR process, metals such as Pt, Pd and Ni–Sn alloys showed higher selectivities towards hydrogen when compared to Ni, Ru and Rh, which tend to make more alkanes and very less hydrogen.

Elliott et al. [15] tested several base and noble metal catalysts for the conversion of p-cresol in subcritical water (350 °C and ~200 bar) and identified Ni, Ru and Rh to be the most active metals for the reaction, but catalyst stability was a major problem. However, Ru was reported to be relatively stable catalyst for C–C bond breaking under hydrothermal conditions but almost complete conversion to methane rich gas was observed in the case of ethylene glycol [14]. Byrd et al. [16] also studied the catalytic properties of Ru/Al_2O_3 for supercritical reforming of glycerol at 750–800 °C and found full conversion using a 40 wt% glycerol solution, but also observed the formation of considerable amounts of undesired methane. Kersten et al. [17] observed full conversion for reforming of a 17 wt% glucose solution to methane rich product gas at 600 °C using a 3 wt% Ru/TiO_2 catalyst.

Ni based catalysts have been frequently explored for gasification of oxygenates (glucose, phenol, methanol) under supercritical conditions [5,18–20]. Ni based catalysts are generally active for gasification, but often tend to deactivate due to sintering and or coke formation [5,18]. Selectivities to hydrogen and methane vary significantly in the studies reported and the choice of support seems to have a strong influence [21]. An unsupported Ni metal wire gave high hydrogen selectivities when methanol was used as reactant [18].

Under subcritical conditions $Pt/\gamma\text{-}Al_2O_3$ is reported to be a stable catalyst showing high activity and selectivity towards hydrogen formation for APR of different model oxygenates, namely methanol, ethylene glycol, glycerol and sorbitol [4,8,13]. One of the key steps in the APR reaction is the dehydration of oxygenates, which typically leads to hydrocarbon based species [13].

Bio-liquids (aqueous phase of bio-oil for example) typically contain oxygenate concentrations in the range of 15–20 wt%. It was already reported that, under supercritical reaction conditions, the reforming of a solution containing at least 15 wt% oxygenate is required to be economically viable under supercritical conditions [22]. The target of this study is the development of an efficient catalyst for maximizing hydrogen yields during reforming of a typical oxygenate such as ethylene glycol taking advantage of the beneficial effects of high reaction rates in supercritical water. Catalyst design should take into account minimization of alkane selectivity which can be caused by dehydration of oxygenates as well as C–O bond hydrogenolysis, *i.e.*, methanation. Further, minimizing coke formation and catalyst deactivation is of importance for practical applications.

Based on the information available for subcritical reforming and discussed above in terms of H_2/CH_4 selectivities and maximizing hydrogen yields, three monometallic catalyst systems Pt, Ir and Ni were chosen for the reforming of ethylene glycol as a model oxygenate in supercritical water. Development of a bimetallic Pt–Ni catalyst for the efficient production of hydrogen from ethylene glycol is discussed.

2. Experimental

2.1. Catalyst preparation

Extrudates of γ-alumina (BASF AL-3992) were crushed and sieved to obtain particles within a size range of 300–600 μm and were used as catalyst support. $H_2PtCl_6{\cdot}6H_2O$, $IrCl_4$ and $Ni(NO_3)_2{\cdot}6H_2O$ precursors (analytical grade > 99.9%) were obtained from Alfa Aesar. Mono- and bi-metallic catalysts were prepared by wet (co) impregnation. The desired amount of precursor(s) was dissolved in water and added to the γ-alumina support (weight ratio H_2O/alumina = 1.8). The water was evacuated under vacuum at 100 °C. Catalysts made with Cl containing precursors were treated at 100 °C for 5 h (10 °C min^{-1}) under hydrogen (100 ml/min H_2 and 100 ml/min N_2) to remove any residual Cl [23]. Materials were finally calcined at 500 °C for 15 h (10 °C min^{-1}) under air (200 ml/min).

2.2. Catalyst characterization

Metal loadings on the γ-alumina support were determined using a Philips X-ray fluorescence spectrometer (PW 1480). Surface areas of the catalysts were measured applying the BET method on an ASAP 2400 (Micromeritics). Metal dispersions were determined with pulse CO chemisorption at room temperature on 100 mg of catalyst using a Micromeritics Chemisorb 2750. CO/M ratios of 1 were assumed for all the catalysts. Before pulsing, the catalyst was reduced in H_2 at 400 °C for 1 h and cooled down in helium to room temperature subsequently. Average metal particle sizes for monometallic catalysts were calculated based on dispersion values, assuming hemispherical particle shape. X-ray diffraction (XRD) patterns were collected over the range $2\theta = 20–75°$ on a Philips X'pert device using Cu Kα1 radiation source. X-ray spectra obtained were compared with the JCPDS/ICDD database. Spent catalysts were analyzed by TGA-MS to determine any coke deposits on the surface. Argon with 1, v/v% O_2 was flown over the catalyst while the temperature was increased from 25 to 800 °C. The weight of the catalyst was monitored by TGA and the composition of the gas output was analyzed by MS. TEM imaging and temperature programmed reduction (TPR) was further used to characterize the catalysts. Catalysts (100 mg) studied by TPR were first heated up to 500 °C in oxygen (5% O_2/95% He) and then cooled down to room temperature in argon to remove any moisture from the surface. TPR experiments were carried out in a 10 ml/min hydrogen flow (5% H_2/95% Ar) and the temperature was increased to 10 °C min^{-1}. Consumption of hydrogen was taken as measure of reduction and plotted as function of temperature.

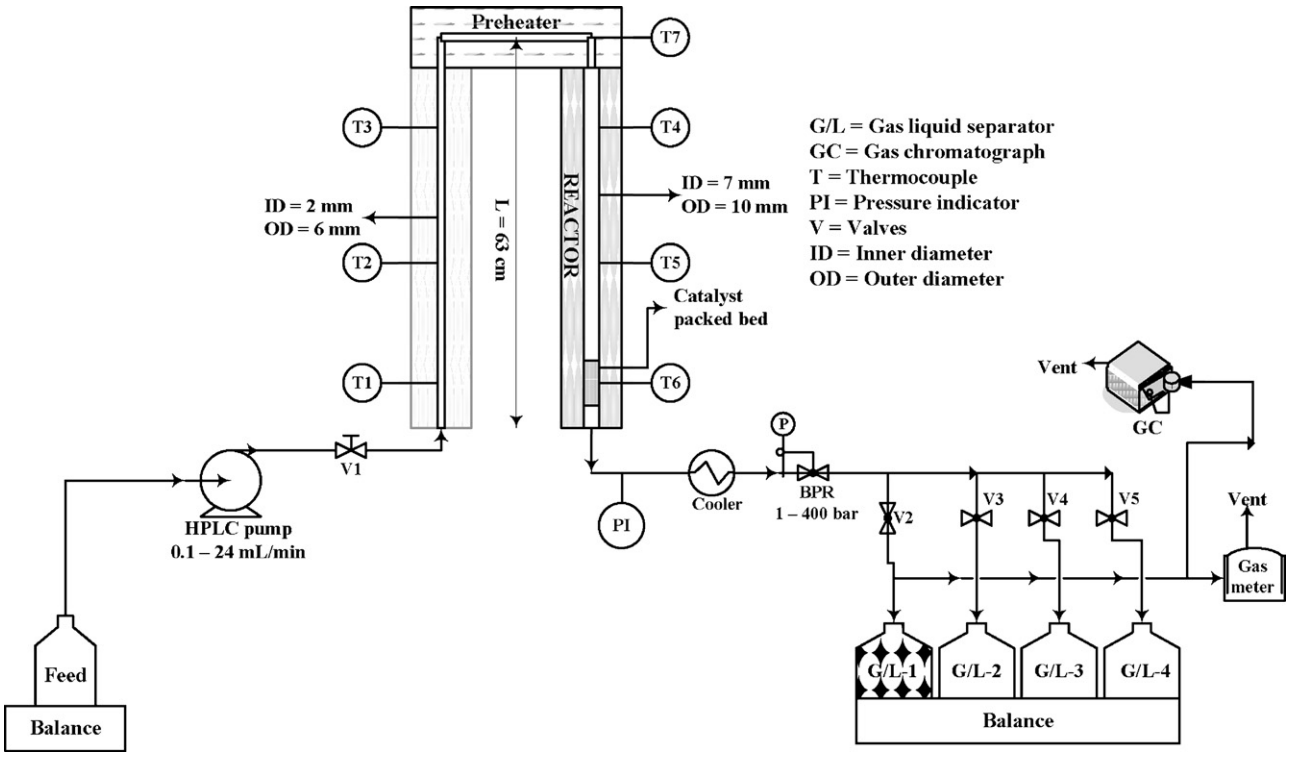

Fig. 2. Schematic representation of the continuous flow supercritical water reformer.

2.3. Catalytic testing

Fig. 2 shows the schematic diagram of the continuous flow supercritical water reformer used in this study. A 2 ml/min flow of ethylene glycol (≥99% Sigma Aldrich) solution (typical concentrations in the range of 5–30 wt% are used depending on the experiment) was preheated to 450 °C at a pressure of 250 bar. After preheating, the solution entered a 63 cm long reactor (ID = 7 mm) in which 1.0 g of catalyst was placed. The reaction was performed at 450 °C and 250 bar. Under these conditions water is in the supercritical regime. The reactor effluent was cooled down to room temperature with a counter-current heat exchanger and pressure was reduced by a back pressure regulator to atmospheric pressure. A 500 ml glass bottle was used to allow the separation of gas and liquid products. The amount of gas produced was measured with an Actaris Gallus 2000 gas meter and the gas composition was analyzed with a Varian CP4900 micro-GC equipped with a MS5 and PPQ column. Carbon content analysis of the feed solution and the liquid product was conducted using an Interscience Flash 2000 Organic Elemental Analyzer. Elemental analyzer was used to determine the unconverted carbon content and HPLC analysis was done to identify the intermediate compounds present in the liquid. The flow rate of the feed stream and the amount of liquid product formed were monitored using balances under the respective glass vessels. Weight hourly space velocities (WHSV, g of ethylene glycol per g of catalyst per h) of EG for reforming of 5 and 15 wt% ethylene glycol solutions were, respectively, 5.9 and 17.8 h^{-1} and the residence time in the catalytic bed was 1.3 s [density of water at reaction conditions (here: T = 450 °C and P = 250 bar) is 109 kg/m^3].

Carbon balance was calculated taking into account the carbon-content in gas and liquid phases. The catalyst performance is presented in terms of selectivities to carbon containing products in gas phase (CO, CO_2, CH_4 and C2+) calculated based on distribution of carbon in these molecules. The carbon to gas conversion calculated have an error margin of ±4%. The maximum amount of hydrogen that can be theoretically obtained includes both reforming and WGS reaction. For ethylene glycol (EG) this maximal reforming ratio (RR) of H_2/CO_2 is 5/2.

$$C_2H_6O_2 \rightarrow 3H_2 + 2CO(\text{optimal reforming})$$

$$2CO + 2H_2O \rightarrow 2CO_2 + 2H_2(\text{WGS})$$

$$C_2H_6O_2 \rightarrow 5H_2 + 2CO_2(\text{overall optimal reaction})$$

$$\%\,H_2 \text{ selectivity} = \frac{H_2 \text{ moles produced}}{\text{C atoms in gas phase}} \frac{1}{RR} \times 100$$

$$\%\,\text{Selectivity of } i = \frac{\text{C atoms in species } i}{\text{C atoms in gas phase}} \times 100,$$

$$\text{where species } i = CO,\ CO_2 \text{ or } CH_4$$

$$\%\,\text{Gasification Efficiency, GE (or) carbon to gas conversion} = \frac{\text{C atoms in gas phase}}{\text{Total C atoms in feed stock}} \times 100$$

Turn over frequencies (TOF) were calculated for the monometallic catalysts based on the metal dispersions and is defined as the number of respective molecules produced/reacted per active catalytic site per minute.

3. Results and discussion

3.1. Catalyst characterization results

Characteristics of the catalysts studied are given in Table 1. All fresh catalysts had surface areas of ±200 m^2/g, similar to that for the alumina used. All catalysts showed decrease in surface areas to ±20 m^2/g during the reaction. This decrease was found to happen during the initial stage of the reaction (within the first 15 min) and also occurred when only water (without organic reactants) was

Table 1
Catalyst characterization results for fresh catalysts.

Catalyst supported on γ-alumina	Loading (%)	Dispersion (%)[a]	Average particle size (nm)	Surface area (m^2/g)
Ni	1.31	1	78	196
Ir	1.41	15	7.2	195
Pt	1.45	68	1.6	196
Pt	0.60	85	1.3	199
Pt	0.30	87	1.2	197
Pt–Ni	1.17–0.33	n.d.	n.d.	198
Pt–Ni	0.60–0.20	n.d.	n.d.	197
Pt–Ni	0.30–0.10	n.d.	n.d.	200

n.d., not determined.
[a] Determined by CO chemisorption.

used. The decreasing surface area can be attributed to phase change of the γ-Al_2O_3 to boehmite as can be seen from the XRD patterns of the fresh and spent 1.15–0.35 wt% Pt–Ni/γ-Al_2O_3 catalysts as shown in Fig. 3. Due to sensitivity issues of XRD, only metal loadings above 5 wt% can be identified. Hence, this technique is used only for identifying transformation of the phase change of γ-Al_2O_3 in supercritical water. For the fresh catalyst, diffraction peaks appear at $2\theta = 45.8^\circ$ and 66.8° which corresponds to γ-Al_2O_3. Multiple peaks emerged for the spent catalyst after exposure to supercritical water and these correspond to the dominant phase of boehmite indicating hydrolysis of the support. Weaker reflections of alpha phase are also noticed. Similar observations of the phase change of γ-Al_2O_3 in supercritical water was reported by many authors [16,24,25]. The phase change occurred during start-up of the reaction and therefore the reactions were performed in the presence of stable catalysts. It was reported earlier by Wawrzetz et al. [26] that the phase change from γ-Al_2O_3 to boehmite did not cause blocking or deactivation of the catalytic sites.

Metal dispersions measured with CO chemisorptions were low for the Ir and Ni catalysts implying large particle sizes of 7.2 nm and 78 nm, respectively. TPR experiment showed that the most dominant Ni species on the support was $NiAl_2O_4$ (no TPR profile presented). A temperature of around 800–1000 °C was necessary to reduce this species under hydrogen at atmospheric pressure. These high reduction temperatures can be the reason for the low Ni dispersions measured, as the $NiAl_2O_4$ could not be reduced under the conditions used for the chemisorption experiment.

The nature of the interactions between Pt and Ni on the bimetallic Pt–Ni catalysts was studied by TPR. Mutual influences between Pt and Ni can vary from (1) no interactions – Pt and Ni are not situated near each other, (2) weak interactions – Pt and Ni are close together and (3) strong interaction – Pt–Ni alloy formation. The TPR profiles of the 0.3 wt% Pt/Al_2O_3, 0.3 wt% Ni/Al_2O_3 and 0.3–0.1 wt% Pt/Al_2O_3 are shown in Fig. 4. Pt/Al_2O_3 showed only one reduction peak at 227 °C which can be attributed to the reduction of $Pt^{IV}(OH)_xCl_y$ to metallic Pt [27]. Ni/Al_2O_3 showed a large reduction peak between 800 °C and 1000 °C which can be attributed to $NiAl_2O_4$ [28]. In the case of the Pt–Ni catalyst, reduction temperatures of 235, 326, 405, 516 and 809 °C were observed. The reduction peak at 809 °C is attributed to $NiAl_2O_4$ [28], indicating that some of the added Ni was inactive during the reaction due to strong interaction with the alumina support. Reduction peaks at 405 and 516 °C indicate large and smaller NiO particles, respectively [29]. The Pt reduction shifted to a higher temperature of 235 °C when Ni was present on the catalyst. This shift is assigned to interactions between Pt and Ni. However, the strength of this interaction is unknown. Also a reduction peak around 326 °C was observed and this is assigned to Ni that is strongly interacting with Pt as Pt is reported to lower the reduction temperature of NiO by facilitating dissociative hydrogen chemisorption which is necessary for the reduction of Ni [30]. Based on the TPR results it can be concluded that various degrees of interaction between Pt and Ni exist on the Pt–Ni catalyst, varying from no interaction to strong interaction.

The monometallic Pt catalysts showed comparatively higher metal dispersion measured by CO chemisorption. A lower dispersion was found for the highest Pt loading, indicating larger particles for the highest Pt loading. Fig. 5A shows a TEM image of the 1.5 wt% Pt on alumina catalyst. EDX confirmed the presence of Pt in this region and dark spots with a sub-nanometer diameter can be seen. These dark spots were not visible in areas were Pt was not indicated by EDX and are therefore attributed to the mass induced contrast between Pt and Alumina. In the case of bimetallic catalysts, determining dispersions separately for Pt and Ni is not straight forward and were not determined. A TEM image of the fresh 1.5 wt% Pt–Ni containing catalyst is shown in Fig. 5B. Again dark spots were

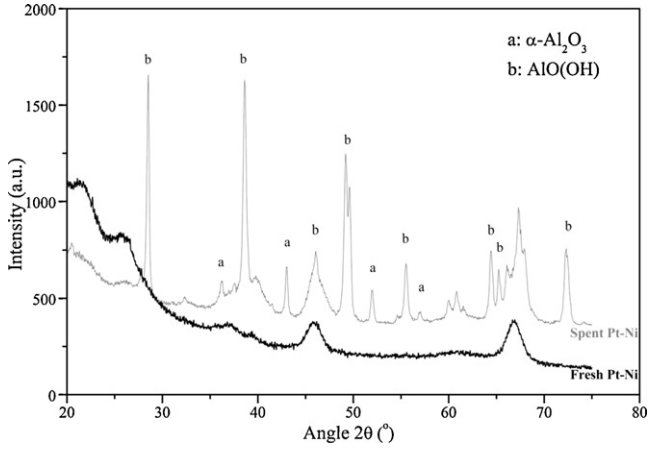

Fig. 3. XRD spectra of fresh Pt–Ni (Pt – 1.15% and Ni – 0.35%) bimetallic catalyst (below) *vs.* spent Pt–Ni catalyst.

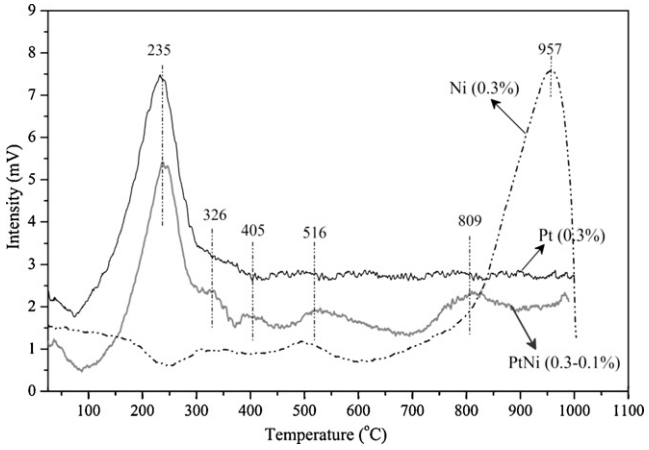

Fig. 4. TPR profiles of fresh catalysts: a) Pt (0.3%) b) Ni (0.3%) and c) Pt–Ni (0.3–0.1%).

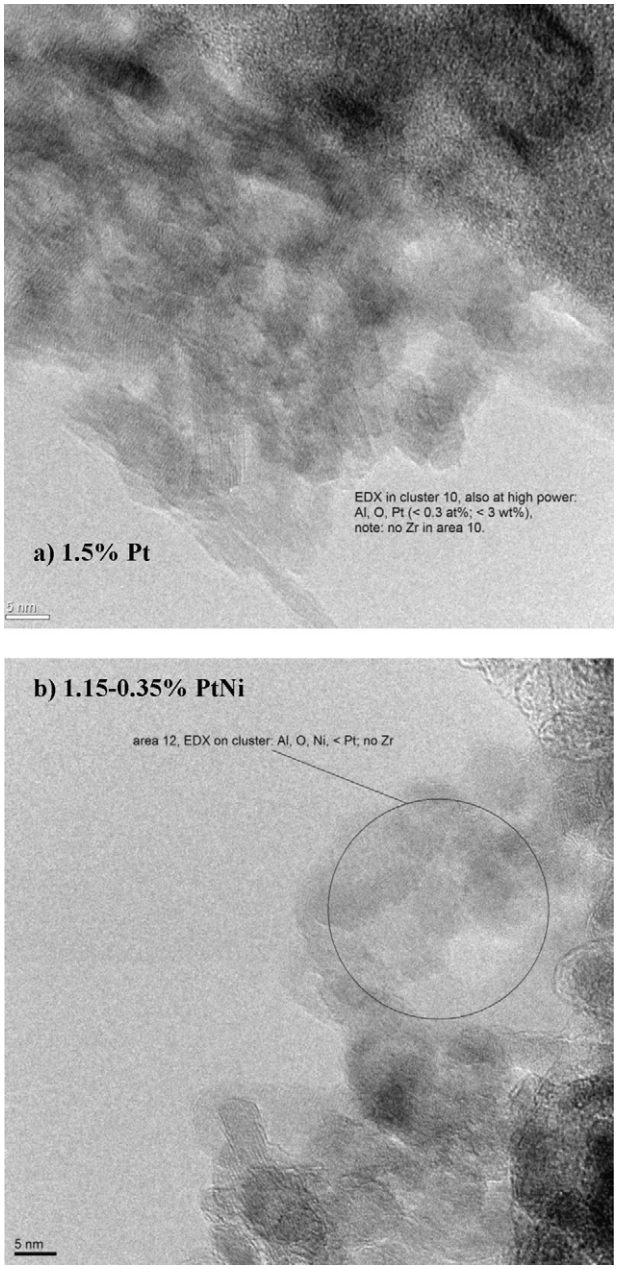

Fig. 5. TEM images (5 nm scale) of fresh (a) 1.5 wt% Pt/γ-Al_2O_3 and (b) 1.15–0.35 wt% Pt–Ni bi-metallic catalysts.

observed on the alumina support. The size of these spots was also sub-nanometer in diameter and is also attributed to Pt or PtNi particles. The presence of only Pt was observed in some areas but Ni was always found together with Pt and shows that Ni deposits in the neighborhood of Pt, indicating interactions between Pt and Ni. TEM imaging indicates that the metal particles (Pt and Pt–Ni) on both catalysts are sub-nanometer in diameter.

3.2. Catalytic reforming results

Thermodynamic equilibrium gas composition [31] of different ethylene glycol concentrations at 450 °C and 250 bar is shown in Fig. 6. Under the reaction conditions used in this study, CH_4 is the favorable product formed with a selectivity of 54% with 5 wt% EG and increases slightly with increasing the feed concentration at the expense of hydrogen.

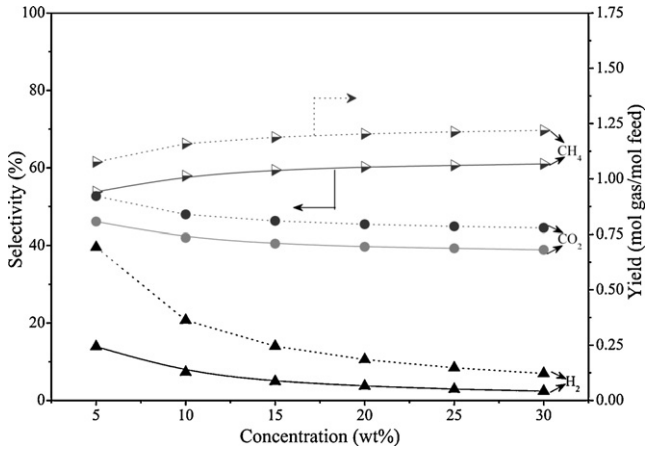

Fig. 6. Thermodynamic chemical equilibrium composition for different feed concentrations ranging from 5 to 30 wt% of ethylene glycol reformed in supercritical water at 450 °C and 250 bar (symbols with solid trend lines represent selectivity and dotted trend lines represent yield).

Results of the catalytic experiments with 5 wt% EG for the alumina supported Ni, Ir, and Pt catalysts, are shown in Table 2. No reforming activity for EG was observed in a blank experiment (no catalyst) or with the alumina support only. In Table 2, carbon to gas (±5%) conversion and carbon remaining in liquid (±2%) indicate good carbon balances (102% and 106%), except for the Ir catalyst where ±30% is deposited on the catalyst as coke. Carbon to gas conversion is taken as measure for the gasification activity. Remaining carbon from the feed is either in coke or in the liquid product (EG, plus other carbon containing species). Results in Table 2 show that at comparable metal loadings, Pt was the most active.

The Ni based catalyst showed the lowest carbon to gas conversion of 6%. Ir catalyst gave a conversion of 27%. Pt catalyst showed near complete conversion of EG to gas phase products. These results are in line with Davda et al. [13], who also found Pt to be more active than Ir. In the case of Ni catalyst, we have used a low loading of 1.5 wt% for comparison with the other catalysts in the study. Other studies report usually much higher Ni loadings (~20 wt%). These catalysts were initially very active but underwent rapid catalyst deactivation. It is therefore difficult to compare our results with these studies [5,13].

In the case of Ni/Al_2O_3 catalyst, NiO clusters formed during calcination can undergo strong interaction with the alumina support, leading to the formation of stable $NiAl_2O_4$. Steam reforming and water gas shift activity is related to the presence of reduced Ni metal particles. The $NiAl_2O_4$ phase is stable under most reforming

Table 2
Experimental data for the reforming of 5 wt% ethylene glycol (WHSV 5.9 h^{-1}) at 450 °C and 250 bar using 1.5 wt% Ni, Ir and Pt supported on γ-alumina.

	1.5 wt% Ni	1.5 wt% Ir	1.5 wt% Pt
Carbon to gas (%)	6	27	100
Carbon in liquid (%)	96	45	6
Selectivity (%)			
H_2	26	35	87
CO_2	31	30	94
CO	55	40	1
CH_4	1	24	4
C2+	13	6	1
Yield (mol gas/mol feed)			
H_2	0.08	0.61	4.24
CO_2	0.04	0.20	1.78
CO	0.06	0.29	0.01
CH_4	0.00	0.18	0.07
C2+	0.00	0.01	0.01

C2+ gases include C_2H_4, C_2H_6, C_3H_6 and C_3H_8.

Table 3
Experimental data for the reforming of 5 wt% ethylene glycol (WHSV 5.9 h^{-1}) at 450 °C and 250 bar using 0.3, 0.6 and 1.5 wt% Pt supported on γ-alumina.

	0.3 wt% Pt	0.6 wt% Pt	1.5 wt% Pt
Carbon to gas (%)	95	99	100
Carbon in liquid (%)	4	2	6
Selectivity (%)			
H_2	76	85	87
CO_2	84	87	94
CO	1	1	1
Alkanes (C_xH_y)	15	12	5

Table 4
Experimental data for the reforming of 15 wt% ethylene glycol (WHSV 17.8 h^{-1}) at 450 °C and 250 bar using 0.3 Pt, 0.6 Pt and 1.5 Pt supported on γ-alumina.

Catalyst	0.3 wt% Pt	0.6 wt% Pt	1.5 wt% Pt
Carbon to gas (%)	48	48	42
Carbon in liquid (%)	58	59	61
Selectivity (%)			
H_2	42	51	80
CO_2	50	60	79
CO	20	14	14
Alkanes (C_xH_y)	30	26	7

conditions and does not contribute to catalyst activity. A TPR experiment showed that the most dominant Ni species on the support was $NiAl_2O_4$. Since the Ni concentration is low in our catalyst, this is the only species to be expected. Catalysts containing larger amounts of Ni usually show both NiO and $NiAl_2O_4$ phases [28]. A temperature in the range of 800–1000 °C was necessary to reduce this species under hydrogen. Thus the low activity of the Ni compared to Ir and Pt catalysts is due to the presence of Ni in inactive $NiAl_2O_4$ phase, in this case.

Table 2 also gives selectivities to the various gas products observed. The target in this study is to achieve a high selectivity towards hydrogen (i) by maximizing water gas shift and (ii) by minimizing methane formation. Both the Ni and Pt catalysts showed low selectivities for methane formation (<4%). Low methanation activity (CH_4 < 4%) and high WGS activity (CO/CO_2 = 0.01) (see Table 2) results in the high selectivity for hydrogen (87%) as observed for the Pt catalyst. From Table 1 it is seen that metal dispersions for Pt is about 4 times higher than Ir and this is also reflected in EG conversion. This implies similar intrinsic activities for both Ir and Pt for EG gasification. However, Ir catalyst showed the highest selectivity towards methane (24%) and also showed high amounts of carbonaceous deposits. Based on the results so far Pt/Al_2O_3 shows the best activity, highest selectivity to H_2 and minimal methane formation.

Optimizing the Pt loading without compromising the EG conversion is interesting from an environmental point of view and from the point of cost of Pt. Table 3 shows the result of the influence of Pt loading on the catalyst performance for the reforming of 5 wt% EG. Characterization results of these catalysts are summarized in Table 1.

It can be seen from Table 3 that even using the lowest Pt loading resulted in near complete conversion of EG. Additional experiments with higher EG concentrations (15 wt%) and at higher space velocities (17.8 h^{-1}) were carried out. The results of these experiments are given in Table 4.

As expected, a lower overall conversion for the reforming of 15 wt% EG solution to carbon containing gaseous products was obtained, under comparable conditions. Interestingly, EG conversion levels were found to be in the same range (42–48%) for all the three Pt catalysts.

Hydrogen selectivities were lower in the case of experiments with higher EG concentration (15 wt%). Davda et al. [13,14,32] also reported that a shift towards CO and CH_4 is introduced with increasing ethylene glycol concentrations. Lower concentrations favor hydrogen, while at higher concentrations, increased levels of CO_x, and H_2 cause (hydrogen consuming) consecutive methane formation. This was observed for all the three catalysts. For the two catalysts, 0.3 and 0.6 wt% Pt, hydrogen selectivity is almost half of that for the experiments with lower EG (5 wt%) concentration. The hydrogen selectivity decreases and methane selectivity increases for 15 wt% EG concentration when compared to 5 wt% EG using the catalyst with the lowest Pt loading (0.3 wt%). Interestingly, in the case of the 1.5 wt% Pt catalyst there is only a small increase in methane formation and hydrogen selectivity is unaffected for the higher EG concentration. HPLC analysis of the effluent obtained with catalyst with 0.3% Pt loading indicated the presence of ethylene glycol and other intermediates compounds such as acetaldehyde, formic acid and very little amount of ethanol.

The intrinsic rates for reforming and hydrogen formation, in the case of experiments with 15 wt% EG, were calculated for the three monometallic Pt catalysts and are summarized in Table 5. Apparent TOF for the reforming of ethylene glycol was found to be more than four times higher for the 0.3 wt% Pt loadings compared to the 1.5 wt% Pt loading. The higher activity (TOF) of the former can be a consequence of (1) Pt particle structure effect (in this case smaller particles are more active) and (2) the higher Pt dispersion in bi-functional catalysts. It has been reported earlier [21] that the boundary between alumina and Pt is thought to be the active catalytic area for reforming since alumina also plays a role in the reforming reaction. Reforming and WGS reactions involve oxidation with the oxygen present in the water molecule. This should involve splitting/activation of water molecules [33]. Pt is normally inert for water activation under typical gasification conditions [34]. Alumina, on the other hand is able to activate water by forming hydroxyl groups, which is necessary for the reforming reaction. Therefore reactive Pt sites should be in close proximity of alumina. Decreasing the particle size will increase the amount of Pt sites neighboring alumina and therefore increasing the overall reforming activity [33].

However, the increase in EG TOF is not proportional with the increase in H_2 TOF (4 *vs.* 2). Results in Table 4 seem to indicate that lower Pt loadings tend to favor methane formation. Lehnert and Claus [25] showed that, for the aqueous phase reforming of glycerol, the reaction was structure sensitive for Pt/Al_2O_3 catalysts. They observed that the selectivity towards CO and CH_4 increased with decreasing Pt particle size. They suggest that smaller particle sizes have more steps in the structure and this favors CO and CH_4 formation. C–C scission is suggested to occur on the face atoms while C–O scission is favored on steps and edges [25]. Thus, in full agreement with the former, smaller Pt particle size can be responsible for the increase in methane formation.

Conditions during reforming in supercritical water are aggressive therefore, catalyst deactivation is a serious issue and lifetimes

Table 5
TOF's for the reforming of 15 wt% ethylene glycol (WHSV 17.8 h^{-1}) and hydrogen production.

Pt loading (%)	Dispersion (%)	Average particle size (nm)	TOF EG 15 wt% EG (min^{-1})	TOF H_2 15 wt% EG (min^{-1})
0.30	87	1.2	173	359
0.60	85	1.3	87	219
1.45	68	1.6	41	163

Table 6
Stabilities of Pt catalysts for the reforming of 15 wt% ethylene glycol (WHSV 17.8 h^{-1}).

Catalyst	Time (h)	Conversion (%)	Selectivity (%)				
			H_2	CO_2	CO	CH_4	C+
0.3	0.5	48	42	50	20	22	8
Pt	9.0	31	72	57	36	5	3
0.6	0.5	48	51	60	14	19	7
Pt	9.0	36	73	66	22	8	4
1.5	0.5	42	80	79	14	4	3
Pt	9.0	42	82	80	15	2	3

can be short due to leaching, sintering (Ostwald ripening) of metal particles and coking. The stability of the catalyst is therefore very critical for practical applications.

The EG conversions to gas phase products and selectivities for the three monometallic Pt catalysts during a 9 h life test are shown in Table 6 for the reforming of 15 wt% EG. The Pt catalyst with the highest Pt loading (1.5 wt%) showed stable performances with respect to activity (42%) and selectivities (H_2 selectivity of 80%) during 9 h on stream. Lower Pt loadings were less stable. For the lowest Pt loading (0.3 wt%) initially a conversion of 48% was obtained. The conversion however gradually dropped to 31% after 9 h on stream. With deactivation hydrogen selectivity improved at the expense of lower CH_4 formation.

One reason for deactivation can be the loss of metal from the catalyst by leaching. XRF analysis of the liquid products showed, however, no presence of metals. In addition metal loadings for the fresh and spent catalysts were found to be the same, verifying that leaching of Pt and alumina support during the reaction was unlikely.

Deactivation by coke deposition is also unlikely as oxidation and re-use of a spent 0.3 wt% Pt/Al_2O_3 catalyst showed. The catalyst was taken out of the reactor after 9 h on stream for the reforming of 15 wt% EG. The spent catalyst was re-oxidized in air at 500 °C for 5 h to burn off any coke species. After this treatment the catalyst was again used for the reforming of 15 wt% EG and no changes in activity or selectivities were observed compared to the properties after 9 h on stream. This indicates that deactivation was not induced by coke deposition. TGA-MS analysis of the spent Pt and Pt–Ni catalysts all showed 12 ± 1% weight loss at 513 ± 3 °C. The gas stream showed that the weight loss was mainly due to the release of H_2O. For all catalysts, release of comparable quantities of water was observed. H_2O is probably formed during recombination of hydroxyl groups on the alumina support. Presence of coke on the catalysts was not indicated by the TGA-MS technique.

An indication for deactivation can be inferred from the selectivity data presented in Table 6. With deactivation the selectivity towards hydrogen improved and methane formation decreased. As discussed earlier [25] the Pt particle size is believed to influence the reforming activity and selectivity towards hydrogen and methane. Larger Pt particles tend to favor the formation of hydrogen, but are less active for EG reforming in contrast to smaller Pt particles that are very active for EG reforming but favor the formation of methane. In line with these arguments we suggest that the dominating deactivation mechanism is due to Pt particle growth. Initially the catalyst showed a high activity and a higher selectivity towards methane. During the reaction the Pt particles are believed to grow, resulting in a lower reforming activity and increased selectivity towards H_2. We can only suggest that the relatively large Pt particle size in the catalyst with the highest Pt loading is the reason for the stability with time.

From the results discussed so far we have shown that full conversion of a 5 wt% ethylene glycol solution to gas phase products could be achieved with high selectivity towards hydrogen using alumina supported Pt catalysts. At the higher EG concentrations (15 wt%) a loss of hydrogen was observed at the expense of more methane formation. Using lower Pt loadings showed a negative effect on the hydrogen selectivity for the reforming of 15 wt% ethylene glycol solution. In addition the catalyst with lower Pt loadings deactivated during the reaction. The 1.5 wt% Pt/Al_2O_3 showed to be the best catalyst in terms of stability and hydrogen selectivity for the reforming of 15 wt% ethylene glycol. However, the intrinsic activity of the Pt active sites was still low.

Reforming of solutions with high EG concentrations and high hydrogen selectivities are economically interesting but this requires modification of the Pt catalysts as seen above. In case of the catalysts with lower Pt loadings the hydrogen selectivity and

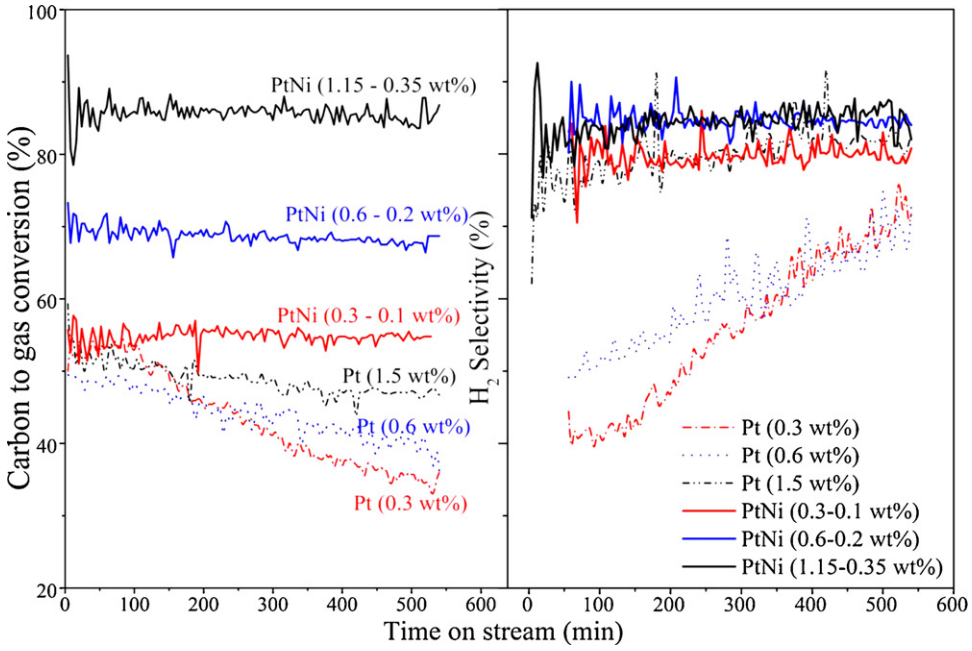

Fig. 7. Activity and stability of monometallic Pt and bi-metallic Pt–Ni catalysts for the reforming of 15 wt% EG at 450 °C and 250 bar.

Table 7
Stabilities of Pt–Ni catalysts for the reforming of 15 wt% ethylene glycol (WHSV 17.8 h^{-1}).

Catalyst	Time (h)	Conversion (%)	Selectivity (%)				
			H_2	CO_2	CO	CH_4	C+
0.3–0.1	0.5	50	77	77	18	4	1
Pt–Ni	9.0	50	79	78	17	3	1
0.6–0.2	0.5	63	84	88	8	3	1
Pt–Ni	9.0	60	85	88	8	3	1
1.15–0.35	0.5	79	83	91	3	4	1
Pt–Ni	9.0	77	86	90	5	4	1

stability should be addressed. For the catalyst with the highest Pt loading the intrinsic activity should be improved. Ni/Al_2O_3 was not a very interesting catalyst with respect to EG conversions and H_2 yields, although Ni/Al_2O_3 showed the lowest CH_4 formation rate. Thus, Ni addition to monometallic Pt catalysts can be expected to improve hydrogen yields. Huber et al. [8] already reported that addition of Ni to a Pt/Al_2O_3 catalyst significantly increased the H_2 selectivity by suppressing CH_4 formation and at the same time also enhanced EG reforming activity. Furthermore, Ni is also an active metal for steam reforming and for the water gas shift reaction (necessary to enhance hydrogen yields) and is a cheaper substitute for Pt [35,36]. Possible synergetic effects of Ni addition to Pt catalysts were investigated for the reforming of ethylene glycol in supercritical water.

Details of the Pt catalysts modified with Ni are given in Table 1. The conversions and selectivities for the three Pt–Ni bi-metallic catalysts are shown in Table 7 for the reforming of 15 wt% ethylene glycol. Addition of Ni induced a significant improvement on the performance of the catalyst. In contrast to the 0.3 wt% Pt catalyst (Table 6) no deactivation was observed with the 0.3–0.1 wt% Pt–Ni catalyst during 9 h on stream. All Pt–Ni catalysts showed stable conversions and selectivities for the reforming of 15 wt% EG during 9 h on stream.

Another positive effect was observed on the hydrogen selectivity by addition of Ni. All tested Pt–Ni catalysts showed high

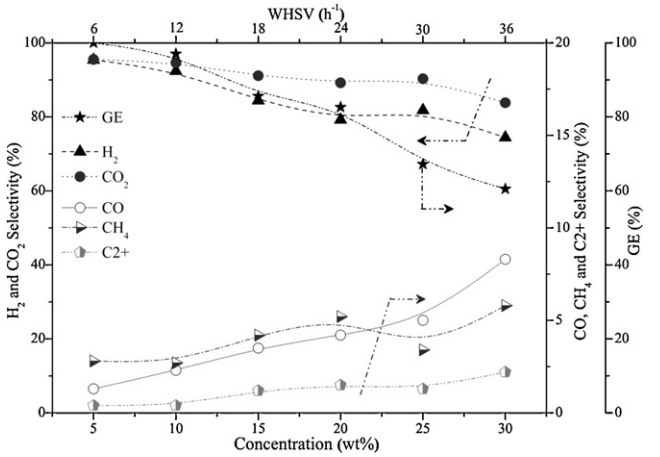

Fig. 8. The influence of ethylene glycol concentration and its corresponding space velocities on the product gas selectivity and gasification efficiency in the presence of Pt–Ni (Pt – 1.15 wt%, Ni – 0.35%) bimetallic catalyst at 450 °C and 250 bar (arrows indicate axis direction).

H_2 selectivities with remarkably low CH_4 selectivities (maximum 3–4%). Addition of Ni to the catalyst with lowest Pt loading (0.3–0.1 Pt–Ni) almost doubled the hydrogen selectivity as a result of suppressing methane formation. In the case of Pt and Pt–Ni catalysts comparable initial concentrations of CO were observed. In case of Pt–Ni catalyst the CO_2 concentrations are much higher compared to the mono-metallic Pt catalyst. This is an indication that in presence of Ni, CO underwent a water gas shift reaction instead of a methanation reaction. The role of Ni in that case is to prevent hydrogenation of CO_x due to the intrinsic water gas shift activity of Ni.

Noble metals such as Pt are not capable of activating water for the water gas shift reaction and therefore require an active support material (in this case alumina) that provides the water activation. Ni however is capable of both activating water and CO in the water gas shift reaction without the need for a support. This occurs *via* NiO

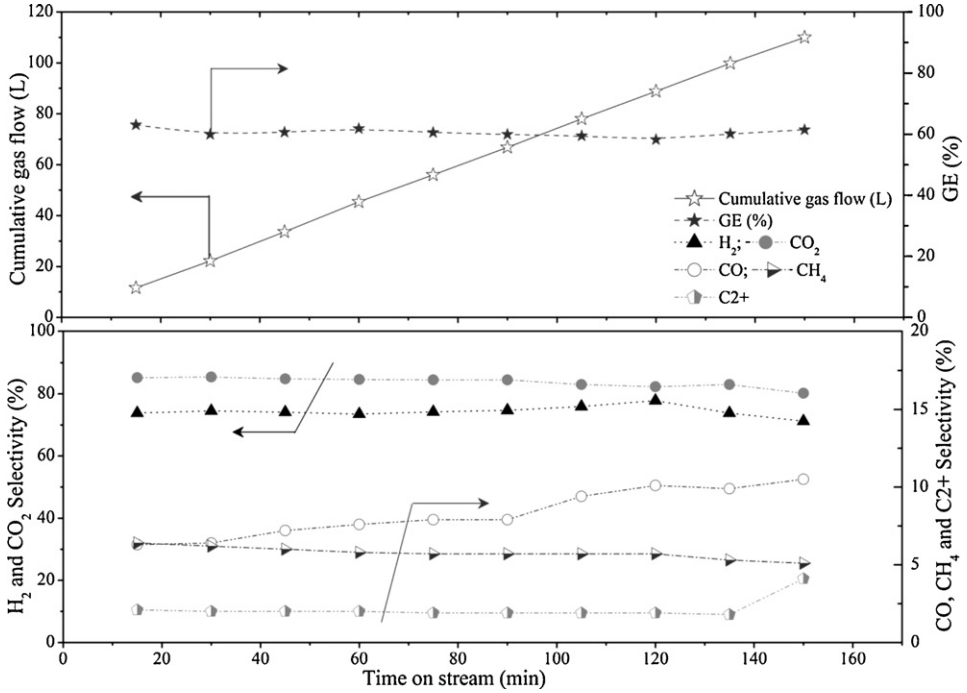

Fig. 9. The gasification efficiency and the product gas selectivity of 30 wt% ethylene glycol concentration versus time with Pt–Ni (Pt – 1.15 wt%, Ni – 0.35%) bimetallic catalyst at 450 °C and 250 bar (arrows point towards axis direction).

formation with water [37]. This intrinsic water gas shift activity of Ni might be the reason for the synergetic effect observed in bimetallic Pt–Ni catalysts.

Remarkably, from Table 7, it can be seen that 1.15–0.35 wt% Pt–Ni catalyst is two times as active as the monometallic counterpart (1.5 wt% Pt) with very high selectivity towards hydrogen (86%). The catalyst is also very stable. Based on calculations, Huber et al. [8] speculated that Pt–Ni catalysts have lower heats of H_2 and CO adsorption compared to pure Pt catalysts, causing lower surface coverage of adsorbed H_2 and CO and therefore minimize methanation of CO and allowing more sites to be accessible for the reactant to undergo reforming.

The carbon to gas conversion of 15 wt% EG and the hydrogen selectivities for the three monometallic Pt catalysts and three bimetallic Pt–Ni catalysts with different metal loadings during a 9 h reaction time is shown in Fig. 7. It is evident from the figure that the bi-metallic catalysts are shown to have higher conversions and stable hydrogen selectivities than the monometallic catalysts.

The influence of EG concentration ranging from 5–30 wt% on the product gas selectivity and gasification efficiency with Pt–Ni (Pt – 1.15% and Ni – 0.35%) is shown in Fig. 8. The carbon to gas conversion decreased from 100 to 60% with increasing concentration from 5 to 30 wt% suggesting that decreasing the space velocity (either by increasing the amount of catalyst or decreasing the feed flow) should give complete conversion at high EG concentrations. The H_2 and CO_2 selectivities decreased while the CO, CH_4 and C2+ selectivities increases with the EG concentration. However, with 30 wt% EG concentration, the carbon to gas conversions remained constant during 3 h experimental run but the CO selectivity increased marginally indicating a decrease in water gas shift activity (Fig. 9).

The bimetallic Pt–Ni/Al_2O_3 catalyst studied here, shows extremely good activity, is stable and very selective to hydrogen. This catalyst shows promise for practical applications. Supercritical water is Brønsted acidic and can be expected to help acid–base catalyzed reactions. This should enhance dehydration of oxygenates leading to reaction intermediates. The role for intermediates formed during dehydration and possible routes from them to hydrogen need to be established. The exact nature of interaction between Pt and Ni are under study in order to establish catalyst requirements.

4. Conclusions

In this article, we studied the catalytic properties of alumina supported Pt, Ir and Ni catalysts for the reforming of ethylene glycol under supercritical conditions. In the case of monometallic Pt catalysts, smaller Pt particles tend to give higher intrinsic activities. This is due to reforming being bi-functional over supported Pt catalysts, the support having the role of water activation. Thus the small particle sizes have larger interfacial (metal/support) area providing a higher activity. However, they yield also lower hydrogen selectivities due to increased methane formation. Methane can be formed by either dehydration of EG, and/or by the hydrogenation of CO_x. A new developed Pt–Ni bimetallic catalyst shows enhanced hydrogen yields by suppressing methane formation. Due to supposed lower CO coverage caused by the presence of Ni and an enhanced accessibility to Pt sites for reforming, the new Pt–Ni catalyst also shows two times more activity compared to a monometallic Pt catalyst. Moreover, the addition of Ni also prevented further sintering of Pt particles and stable performances were observed for the bimetallic Pt–Ni catalysts for the reforming of ethylene glycol even under supercritical conditions.

Acknowledgements

This project was funded by the EOS-LT program of SenterNovem (EOS-LT 05020) and ACTS (project number 053.61.023). The authors greatly acknowledge Louise Vrielink for BET and XRF analysis. Karin Altena is acknowledged for dispersion measurements. Benno Knaken and Bert Geerdink are acknowledged for their technical support.

References

[1] M.F. Bleeker, S.R.A. Kersten, H.J. Veringa, Catalysis Today 127 (1–4) (2007) 278–290.
[2] Y. Kalinci, A. Hepbasli, I. Dincer, International Journal of Hydrogen Energy 34 (21) (2009) 8799–8817.
[3] A. Tanksale, J.N. Beltramini, G.M. Lu, Renewable and Sustainable Energy Reviews 14 (1) (2010) 166–182.
[4] R.D. Cortright, R.R. Davda, J.A. Dumesic, Nature 418 (6901) (2002) 964–967.
[5] Y. Guo, S.Z. Wang, D.H. Xu, Y.M. Gong, H.H. Ma, X.Y. Tang, Renewable and Sustainable Energy Reviews 14 (1) (2010) 334–343.
[6] S. Czernik, R. French, C. Feik, E. Chornet, Industrial & Engineering Chemistry Research 41 (17) (2002) 4209–4215.
[7] J.W. Shabaker, R.R. Davda, G.W. Huber, R.D. Cortright, J.A. Dumesic, Journal of Catalysis 215 (2) (2003) 344–352.
[8] G.W. Huber, J.W. Shabaker, S.T. Evans, J.A. Dumesic, Applied Catalysis B: Environmental 62 (3–4) (2006) 226–235.
[9] Y. Matsumura, T. Minowa, B. Potic, S.R.A. Kersten, W. Prins, W.P.M. van Swaaij, B. van de Beld, D.C. Elliott, G.G. Neuenschwander, A. Kruse, M. Jerry Antal jr., Biomass and Bioenergy 29 (4) (2005) 269–292.
[10] A. Yamaguchi, N. Hiyoshi, O. Sato, K.K. Bando, M. Osada, M. Shirai, Catalysis Today 146 (1–2) (2009) 192–195.
[11] M.H. Waldner, F. Krumeich, F. Vogel, The Journal of Supercritical Fluids 43 (1) (2007) 91–105.
[12] E.C. Vagia, A.A. Lemonidou, International Journal of Hydrogen Energy 32 (2) (2007) 212–223.
[13] R.R. Davda, J.W. Shabaker, G.W. Huber, R.D. Cortright, J.A. Dumesic, Applied Catalysis B: Environmental 43 (1) (2003) 13–26.
[14] R.R. Davda, J.W. Shabaker, G.W. Huber, R.D. Cortright, J.A. Dumesic, Applied Catalysis B: Environmental 56 (1–2) (2005) 171–186.
[15] D.C. Elliott, T.R. Hart, G.G. Neuenschwander, Industrial & Engineering Chemistry Research 45 (11) (2006) 3776–3781.
[16] A.J. Byrd, K.K. Pant, R.B. Gupta, Fuel 87 (13–14) (2008) 2956–2960.
[17] S.R.A. Kersten, B. Potic, W. Prins, W.P.M. van Swaaij, Industrial & Engineering Chemistry Research 45 (12) (2006) 4169–4177.
[18] G.J. DiLeo, P.E. Savage, The Journal of Supercritical Fluids 39 (2) (2006) 228–232.
[19] T. Furusawa, T. Sato, H. Sugito, Y. Miura, Y. Ishiyama, M. Sato, N. Itoh, N. Suzuki, International Journal of Hydrogen Energy 32 (6) (2007) 699–704.
[20] I.-G. Lee, S.-K. Ihm, Industrial & Engineering Chemistry Research 48 (3) (2008) 1435–1442.
[21] J.W. Shabaker, G.W. Huber, R.R. Davda, R.D. Cortright, J.A. Dumesic, Catalysis Letters 88 (1) (2003) 1–8.
[22] A. Nakamura, E. Kiyonaga, Y. Yamamura, Y. Shimizu, T. Minowa, Y. Noda, Y. Matsumura, Journal of Chemical Engineering of Japan 41 (8) (2008).
[23] D. Radivojevic, K. Seshan, L. Lefferts, Applied Catalysis A: General 301 (1) (2006) 51–58.
[24] N. Luo, X. Fu, F. Cao, T. Xiao, P. Edwards, Fuel 87 (17–18) (2008) 3483–3489.
[25] K. Lehnert, P. Claus, Catalysis Communications 9 (15) (2008) 2543–2546.
[26] A. Wawrzetz, B. Peng, A. Hrabar, A. Jentys, A.A. Lemonidou, J.A. Lercher, Journal of Catalysis 269 (2) (2010) 411–420.
[27] H. Lieske, G. Lietz, H. Spindler, J. Volter, Journal of Catalysis 81 (1) (1983) 8–16.
[28] C. Li, Y.-W. Chen, Thermochimica Acta 256 (2) (1995) 457–465.
[29] J. Zielinski, Journal of Catalysis 76 (1) (1982) 157–163.
[30] J. Arenas-Alatorre, A. Gomez-Cortes, M. Avalos-Borja, G. Diaz, The Journal of Physical Chemistry B 109 (6) (2004) 2371–2376.
[31] A.G. Chakinala, D.W.F. Brilman, W.P.M. van Swaaij, S.R.A. Kersten, Industrial & Engineering Chemistry Research 49 (3) (2009) 1113–1122.
[32] R.R. Davda, J.A. Dumesic, Angewandte Chemie International Edition 42 (34) (2003) 4068–4071.
[33] K. Takanabe, K. Aika, K. Inazu, T. Baba, K. Seshan, L. Lefferts, Journal of Catalysis 243 (2) (2006) 263–269.
[34] D.C. Grenoble, M.M. Estadt, D.F. Ollis, Journal of Catalysis 67 (1) (1981) 90–102.
[35] B. Matas Güell, I.V. Babich, L. Lefferts, K. Seshan, Applied Catalysis B: Environmental 106 (3–4) (2011) 280–286.
[36] J.H. Lin, P. Biswas, V.V. Guliants, S. Misture, Applied Catalysis A: General 387 (1–2) (2010) 87–94.
[37] J.R. Rostrup-Nielsen, Catalytic Steam Reforming, Springer-Verlag, Berlin/Heidelberg/New York/Tokyo, 1984, ISBN: 3-540-12665-1.